Field Emission of Electrons from Hemispherical Conducting Carbon Nanotube tip including the Effect of Image Force

A Dissertation submitted towards the partial fulfillment of
the requirement for the award of degree of

Master of Technology
in
Nano Science and Technology

Submitted by

Anand Sharma
2K13/NST/10

Under the supervision of

Prof. S.C. Sharma
(HOD, Applied Physics)

Department of Applied Physics

Delhi Technological University
(Formerly Delhi College of Engineering)
Delhi-110042
JULY 2015

DELHI TECHNOLOGICAL UNIVERSITY
Established by Govt. Of Delhi vide Act 6 of 2009
(Formerly Delhi College of Engineering)
SHAHBAD DAULATPUR, BAWANA ROAD, DELHI-110042

CERTIFICATE

This is to certify that work which is being presented in the dissertation entitled **Field Emission of Electrons from Hemispherical Conducting Carbon Nanotube tip including the Effect of Image Force** is the authentic work of **Anand Sharma** under my guidance and supervision in the partial fulfillment of requirement towards the degree of **Master of Technology in Nano Science and Technology**, run by Department of Applied Physics in Delhi Technological University during the year 2013-2015.

As per the candidate declaration this work has not been submitted elsewhere for the award of any other degree.

Prof. S. C. Sharma

Supervisor

H.O.D., Applied Physics

Delhi Technological University,

Delhi

DECLARATION

I, hereby, declare that all the information in this document has been obtained and presented in accordance with academic rules and ethical conduct. This report is my own, unaided work. I have fully cited and referenced all material and results that are not original to this work. It is being submitted for the degree of Master of Technology in Nano Science and Technology at the Delhi Technological University. It has not been submitted before for any degree or examination in any other university.

Signature :

Name :Anand Sharma

ACKNOWLEDGEMENT

I take this opportunity as a privilege to thank all individuals without whose support and guidance I could not have completed my project successfully in this stipulated period of time.

First and foremost I would like to express my deepest gratitude to my supervisor **Prof. S.C. Sharma**, HOD, Applied Physics, for his invaluable support, guidance, motivation and encouragement throughout the period this work was carried out.

I am also thankful to **Ms Aarti Tewari** and **Mr. Ravi Gupta (Research scholars)** for their valuable support and guidance in carrying out this project.

I am deeply grateful to **Dr. Pawan Kumar Tyagi** (Branch coordinator, NST) for his support and encouragement in carrying out this project.

I also wish to express my heartful thanks to staff at Department of Applied Physics of Delhi Technological University for their goodwill and support that helped me a lot in successful completion of this project.

.

Anand Sharma
M. Tech. (NST)
2K13/NST/10

ABSTRACT

The present work examines the field emission from Conducting Hemispherical Carbon Nanotune (CNT) tip including the Effect of Image Force. An expression for electrostatic potential for a Hemispherical CNT tip at a distance from the centre of CNT has been derived. Using the time-independent Schrodinger equation corresponding expressions for transmission coefficient and field emission current density have been derived for the Hemispherical Conducting Carbon Nanotubes. The numerical calculations of potential, transmission coefficient and the current density function have been calculated for a typical set of carbon nanotube parameters. From the expression of potential energy we found that the potential energy for the hemispherical CNT tip first increases and then decreases with the radial distance. The transmission coefficient increases with the normalized radial energy. And the current density function also increases with the normalized Fermi energy. An important outcome of the present work is that both transmission coefficient and field emission current density function decreases as the hemispherical CNT tip radius increases.

.

TABLE OF CONTENTS

CHAPTERS

LIST OF FIGURES

LIST OF TABLES

LIST OF SYMBOLS

V(r)	Potential energy
σ	Surface Charge density
r	Distance from the centre of hemispherical CNT
h	Distance from the surface of hemispherical CNT tip
H	Distance from the base of image hemisphere of CNT
2a	Distance between the center of hemispheres
R	Radius of hemispherical CNT
m_e	Mass of electron
ε_0	Permittivity in free space
β	Field enhancement factor
q	Electric charge
h	Planck's constant
ψ	Wave function
ε_ρ	Normalized radial energy
ε_f	Fermi energy
$T\left(\varepsilon_\rho\right)$	Electron transmission probability
J	Field emission current density
ϕ	Current density function

Chapter 1

Introduction of Carbon Nanotubes

1.1 Introduction

Carbon Nanotubes (CNTs), graphene, buckyballs, graphite and diamond are the structural arrangements of carbon atom. These structural variations depend on the hybridization found in the arrangement. Graphene is the arrangement of carbon atoms in planer form having sp^2 hybridization. CNTs are one-dimensional cylinders having sp^2 hybridized atoms. They also contain some percentage of sp^3 hybridized atoms which is depend on radius of curvature of nanotubes. CNTs are one-dimensional material. Structurally, they are cylindrical folding of graphene sheets. They are either cylindrical arrangement of single graphene sheet (single walled nanotube) or of several coaxial cylinders (multiwalled nanotube) with an interlayer spacing of 3.4 – 3.6 Å. They are the important structure of Nano science and nanotechnology because of their remarkable properties and specific functions. CNTs have high potential applications such as in the field of energy, electronics, medical research like efficient drug delivery and materials. They have gained great interest in research community because of their exotic electronic properties, and this interest continued as other remarkable properties were discovered and promise of practical applications developed.

1.2 Structure of Carbon Nanotubes

Depending on the structure we have classified CNTs into two categories. First belongs to single walled carbon nanotubes, and second category belongs to multi walled carbon nanotubes. Structures of nanotubes are easy to imagine. Fig. 1.1 and Fig. 1.2 shows single walled nanotube and multi walled nanotube, respectively.

1.2.1 Single-Walled Nanotubes (SWNTs)

Geometrically, Single-Walled Nanotubes are cylindrical folding of graphene sheet that are normally capped at the ends. CNTs have hexagonal arrangement of carbon atoms except at the nanotube tip. All carbon atoms are arranged in equivalent position, at the

nanotube tips where 30 atoms at each tip are arranged in pentagonal rings where adjacent pentagons are not unique.

Fig. 1.1 Single Walled Carbon Nanotube

Ideally, the C=C bond angle should be planer, but they are not .The reason for non-planer C=C angle is hybridization of carbon atoms. Carbon atoms in CNTs are no longer pure sp^2 hybridized but have some percentage of sp^3 hybridization. The proportion of sp^3 hybridization increases as the tube radius of curvature decreases.

The minimum diameter of single walled nanotubes which have been synthesized in lab is 0.4 nm. The SWNTs diameter is restricted by its yield in synthesis. The restriction on nanotube length is unlike its diameter. The length of nanotube only depends on the limitations of the preparation method and the experimental conditions used. Generally, Single walled nanotubes have diameter in the range of 1 nm. However, SWNTs have high aspects ratio.

SWNTs can be used in various applications such as in field of electronics and mechanical. For future electronics, nanotechnology is base for Moore's law. In the field of electronics, SWNTs are used as field emission display, logic elements and nanosensors. Also they have tremendous application in mechanical field such as nanocomposite and nanofibers. These materials can play a major role in the next generation of miniaturized electronics. Along with several applications in electronics and mechanical fields, SWNTs are also a famous elements for biological application. One of the important application is biological imaging, which may be used for cancer diagnosis and therapy.

1.2.2 Multi-Walled Nanotubes (MWNTs)

Multi-walled nanotubes can be imagined as a coaxial arrangement of single walled nanotube, similar to coaxial pipes of different radius, or a circular folding of single sheet graphite as shown in Fig. 1.2. The diameters of MWNTs are ranging from 50Å to 500 Å. The interlayer spacing in MWNT is ranging from 3.354Å to 3.44 Å.

Fig. 1.2 Multi Walled Carbon Nanotube

During synthesis, if ambient condition will not be favourable then the regions of structural imperfection may be found. The structural imperfections may diminish its desirable material properties. Synthesis of SWNTs requires relatively extra care. MWNTs are easier to produce in high volume because of less extra care required. Because of high structural complexity of MWNTs, they are less understood. The prices of SWNTs are relatively higher than MWNTs because of extensive care required in synthesis. The performances of SWNTs are ten times better than MWNTs, and some are outstanding for very specific applications.

1.3 Geometrical Structure and Types of nanotube

There are several ways for representing SWNTs by rolling a graphene sheet. Some of the rolled graphene sheet possesses planes of symmetry both parallel and perpendicular with the axis as shown in Fig. 1.3 (a) & (c), while others do not, as shown in Fig. 1.3(b). The non-symmetric folding is commonly called chiral or helical nanotube, since they do not superimposed on their mirror image. Vector of helicity C_h and angle of helicity θ is the mathematical way to represent these folding of graphene sheet as shown in Fig. 1.4.

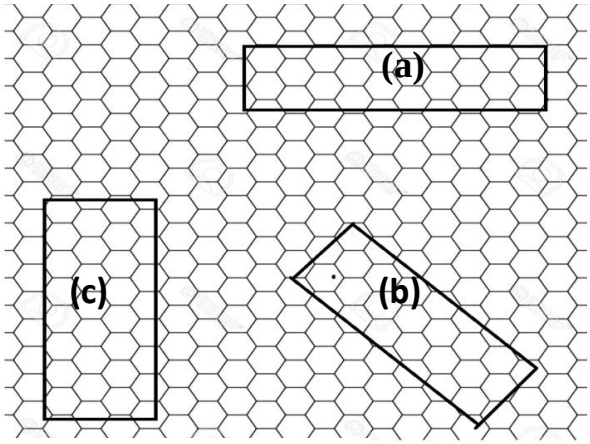

(a) Zigzag-type nanotube

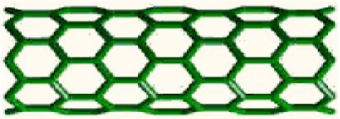

(b) Helical-type nanotube

(c) Armchair-type nanotube

Fig. 1.3 Structure of CNT

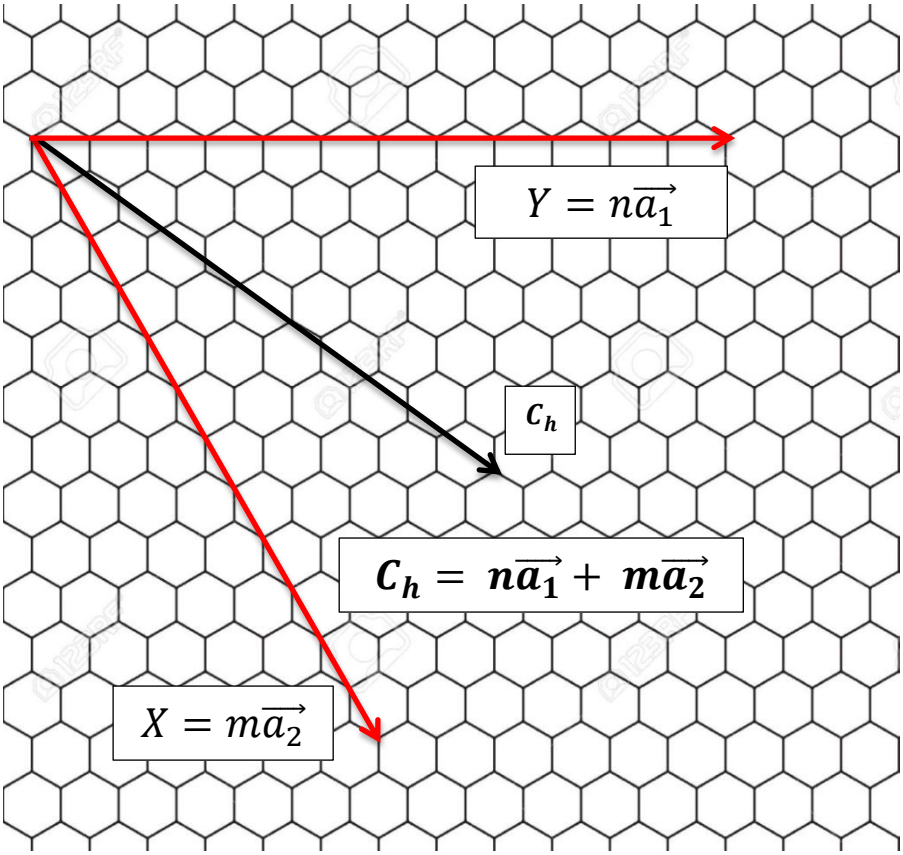

Fig. 1.4 Chiral Vector for CNT

$$C_h = n\overrightarrow{a_1} + m\overrightarrow{a_2}$$

$$\cos\theta = \frac{2n+m}{2\sqrt{n^2+m^2+nm}}$$

where $\overrightarrow{a_1}$ and $\overrightarrow{a_2}$ are primitive lattice vector. n and m are integer : chiral number

$$D = \frac{|C_h|}{\pi} = \frac{a\sqrt{n^2+m^2+nm}}{\pi}$$

where $a = |\overrightarrow{a_1}| = |\overrightarrow{a_2}| = r_o\sqrt{3}$. Here, r_o is bond length of carbon atom.

The C−C bond length is not straight because it is elongated by the curvature imposed by the structure. Helicity angle, θ, and diameter of carbon nanotube D are expressed as a function of the chiral numbers (n, m). So, helicity angle θ *and* diameter of CNT D is sufficient to represent any particular SWNT by assigning them chiral number (n, m). Chiral number (n, m) for given SWNTs can be simply obtained by counting the number of hexagons that separate the extremities of the C_h vector following the primitive lattice vector $\overrightarrow{a_1}$ and then $\overrightarrow{a_2}$.

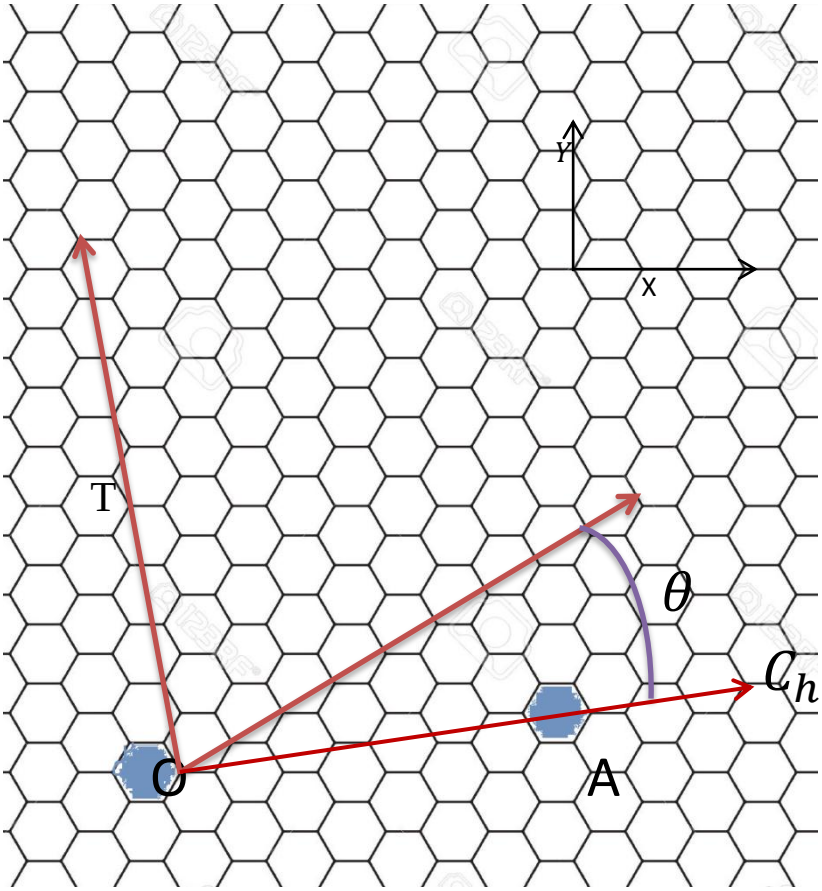

Fig. 1.5 Geometry of carbon nanotube

In zigzag-type SWNTs, the arrangement of carbon atoms is in zigzag form. Zigzag type SWNTs are formed, when helicity vector C_h will be perpendicular to any of the three overall C=C bond directions and helicity angle θ=0, which is denoted by (n, 0) as shown in Fig. 1.5. Armchair-type SWNTs are formed, when helicity vector C_h will be parallel to one of the three C=C bond direction and helicity angle $\theta = \frac{\pi}{6}$, which is denoted by (n, n). Helical SWNTs are obtained when helicity angle when θ lie between 0 to $\frac{\pi}{6}$.

Chapter 2

Properties

2.1 Strength and Elasticity

Graphene is a planer arrangement of carbon atoms. Atoms form a honeycomb lattice. Each atom is connected by via a strong chemical bond to three adjacent atoms. Due to these strong chemical bonds, the basic plane modulus of elasticity of graphene is one of the largest of any known material. This is one of the reason for CNT to be a high-strength fiber. SWNTs are stronger than steel. They are resistant against mechanical forces. Application of mechanical force on the tip of a nanotube will cause it to bend, but without any damage of the nanotube. After removal of force, the nanotube can return to its original state. This property enables CNTs as very useful probe tips for very high-resolution scanning probe microscopy.

2.2 Electrical Conductivity

CNTs possess highly conductive behaviour, and hence it can said to be metallic. The chirality and the degree of twist of tube diameter determine their conductivity. Generally, CNTs behave electrically as a metallic conductor. But some time they also behave as a semi-conducting material. Explanations of conductivity of CNTs are complex phenomena. There is sudden change in transport current at various position in semiconducting SWNTs. The current across metallic single walled nanotube is same, there is no abrupt change in current like semiconducting SWNTs. Performance of some of armchair-type SWNTs are better than metallic MWNTs. Current in MWNTs are redistributed over individual tubes non uniformly. This redistribution of current is due to inter wall reaction within MWNTs.

Conductivity measurement of SWNTs is relatively complex phenomena. It is measured by placing electrode at different position of CNTs. The conductivity of the single walled nanotubes are of the order of 10^4 mho/cm at room temperature (300 K). The possible achieved current density is 10^7 amp/cm^2, however theoretically derived current densities for single walled nanotube is, as high as 10^{13} amp/cm^2. It has been considered that during synthesis of single walled nanotubes defects may be occurred. These defects are advantageous. We can use nanotube as a transistor because of these defects. A nanotube can

also be used as a rectifying diode. One of the interesting and recently reported electrical property is that nanotube can transmit electrical signal between two semiconducting device upto the speed of 10 GHz .

2.3 Field Emission

Emission of electron from metal surface to vacuum requires a strong electric field. But in case of CNT the emission of electron is at lower electric potential. The emission of electron from CNT is possible only due its high aspect ratio (smaller diameter and longer height). This was experimented by de Heer and Co-workers at EPFL in 1995. They immediately realized that these field emitters must be superior to the other conventional electron sources and might find their way into all kind of applications, most important application was in flat-panel displays. Only after five year, a very bright color display was actually realized by Samsung, which will be shortly commercialized using this technology

2.4 Thermal Conductivity

Superconductivity is the phenomena of zero electrical resistance when material is cooled below critical temperature. CNTs also exhibit superconductivity. Characteristics critical temperature for CNT is 20 K. Strong in-plane graphitic carbon - carbon bonds make them very strong and stiff against axial strains. Both, by theoretical and experimental studies it has been prove that the CNTs have high thermal conductivity.

Chapter 3

Theory of Field Emission

3.1 Introduction

Now a days, electron sources have huge application in research and in day today life. Generally, electron emitters are of two types. First one is cold electron emitters and second one is thermionic emitters. Cold electron emitters have principle based field emission of electron. They have potential application for numerous purposes. Although, the application of conventional thermo-electronic emitter seems to be declining. Field emitter should be long, thin and made up of high strength material.

Carbon Nanotubes require very low turn-on field and they have high current density. It was published in first article reporting CNTs properties in 1995. After the publication of this article, CNTs application as field emitter found an edge. First field emission device was presented in 1998. After that the next issue was the large scale production compatibility with micro fabrication technology.

CNTs can be used for emission of single coherent electron beam. Electron microscopy is the device that uses single nanotube for emission of coherent electron beam. Nanotube can also be used in multiple electron beam devices. Multiple electron beam emitter application can be found in flat panel display, where a patterned film of nanotubes provides a large number of electron beams. Every electron beam will be independent of each other.

3.2 Field emission basics

Field emission process is of two types as discussed above. Extraction of electrons in both the processes is from a solid by tunneling process through the surface potential barrier. In field emission of electron the emitted current depends on the local electric field at the emitting surface, E and on its work function, ϕ as shown in Fig. 3.1. Dependency of emitted current on local electric field E and work function, ϕ can be understood with the help of Fowler-Nordhiem (F-N) model as shown below. Fowler-Nordhiem (F-N) equation is an exponential equation.

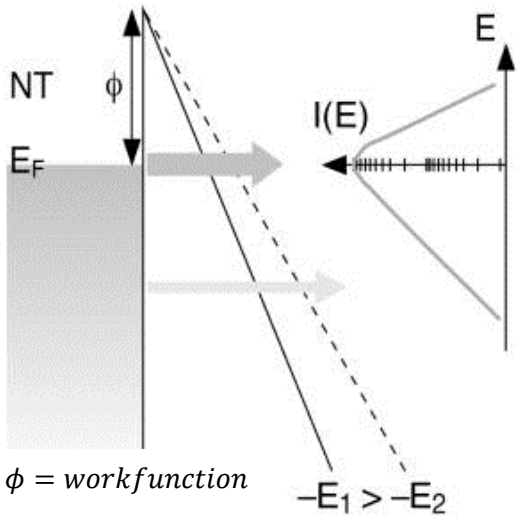

Fig. 3.1 Model for metallic emitter

By quantum mechanical tunnelling, the carriers can pass through the barrier. The first generally accepted explanation of field emission in terms of quantum mechanics is provided by Fowler-Nordhiem (F-N) which they applied for the electronic energy levels in metal to the sommerfeld model. They defined a relationship between the applied electric field and the emission current density.

The Fowler-Nordhiem (F-N) equation for the field emission current density (J) is given by

$$J = \frac{aE_t^2}{\phi} exp\left(\frac{-b\phi^{3/2}}{E_t}\right) ,$$

where

$a = 1.56 \times 10^{-6} AV^{-2}eV$,

$b = 6.83 \times 10^{7} eV^{-3/2}cm^{-1}$,

E_t = Electric field at the tip,

ϕ = Work function,

As E_t is written as βE where E is V/d is the applied field, β is the field enhancement factor and may be written as h / r, where h is the height of the tip and r is the radius of the curvature of the tip. From the above equation we can say that the current density J also depends on shape and surrounding of field emitters.

$$J = \frac{a(\beta E)^2}{\phi} exp\left(\frac{-b\phi^{3/2}}{\beta E}\right)$$

In the form of both single tips and films, field emission properties of MWNTs have been investigated. As nanotubes produce very high current densities and show low operating voltage so they compare very favourably with the other field emission sources.

Chapter 4

An Electrostatic Model For Field Emission

4.1 Introduction

Field emission from CNT tip is interesting phenomena because of its unique behaviour. We have proposed an electrostatic model for field emission from hemispherical carbon nanotube tip. In the proposed model the CNT is perfectly capped at the upper end with hemisphere. We have considered the effect of image charge on field emission. The diagram shown below present the schematic of carbon nanotube. The upper part of CNT is perfectly hemispherical. We know that the major part of field emission is from the tip.

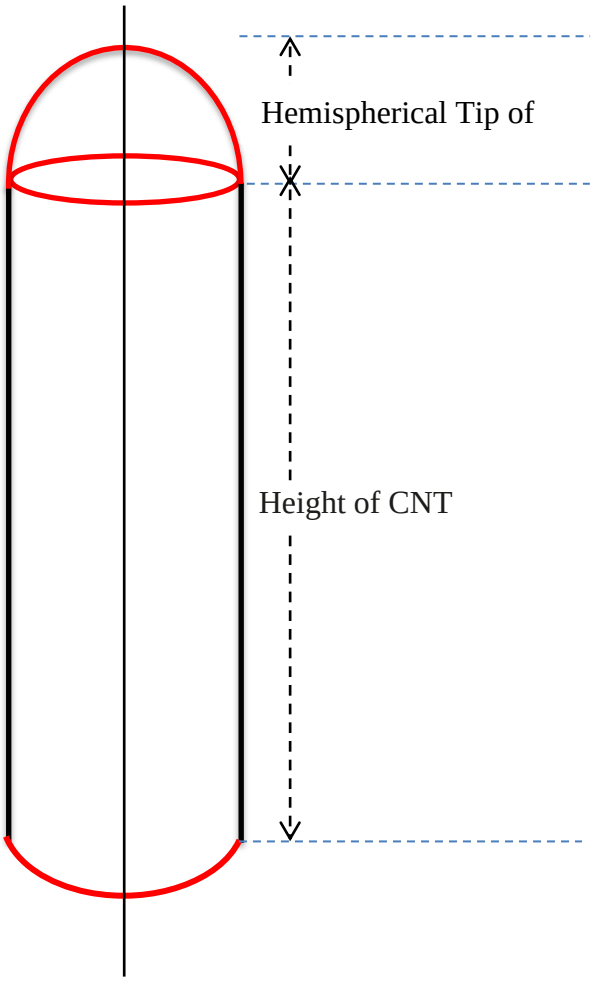

Fig. 4.1 Schematic diagram of CNT

4.2 Model

If we will consider the image charge effect in our calculation then the model for calculation of potential due to hemispherical CNT tip shown in figure below.

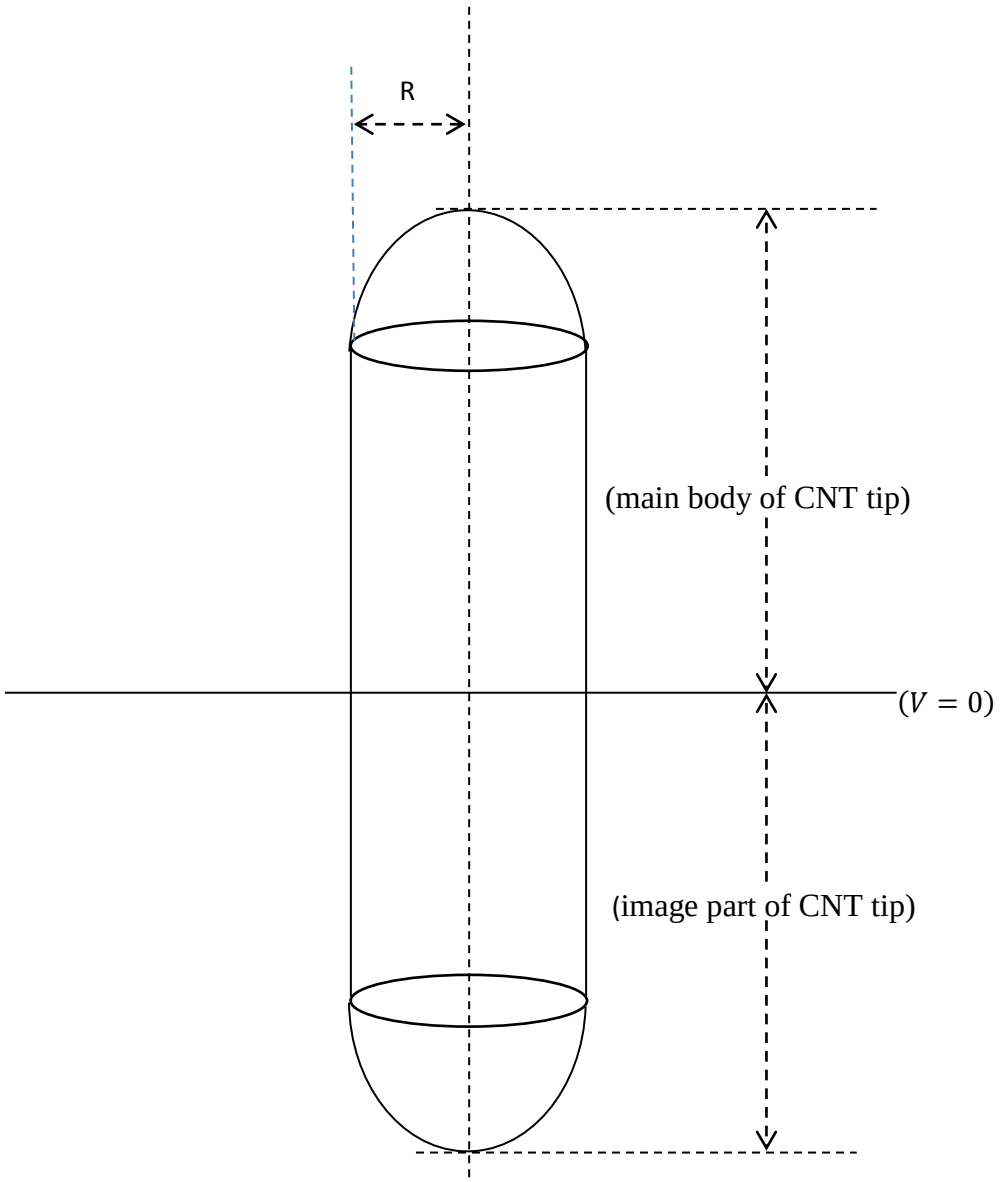

Fig. 4.2 Schematic diagram of CNT with image part

Because the major part of emission is concentrated on the tip of CNTs. Therefore the diagram shown below will explain field emission with precision. First we will find the potential due to upper hemispherical tip and then for lower image part. Fig. 4.3 represents a hemisphere of radius R. For calculation of potential at point $P(0, y, 0)$ we will consider that the hemisphere is made from infinitesimal ring charges. Consider a infinitesimal ring charge of strip width $d\theta$ at an angle θ.

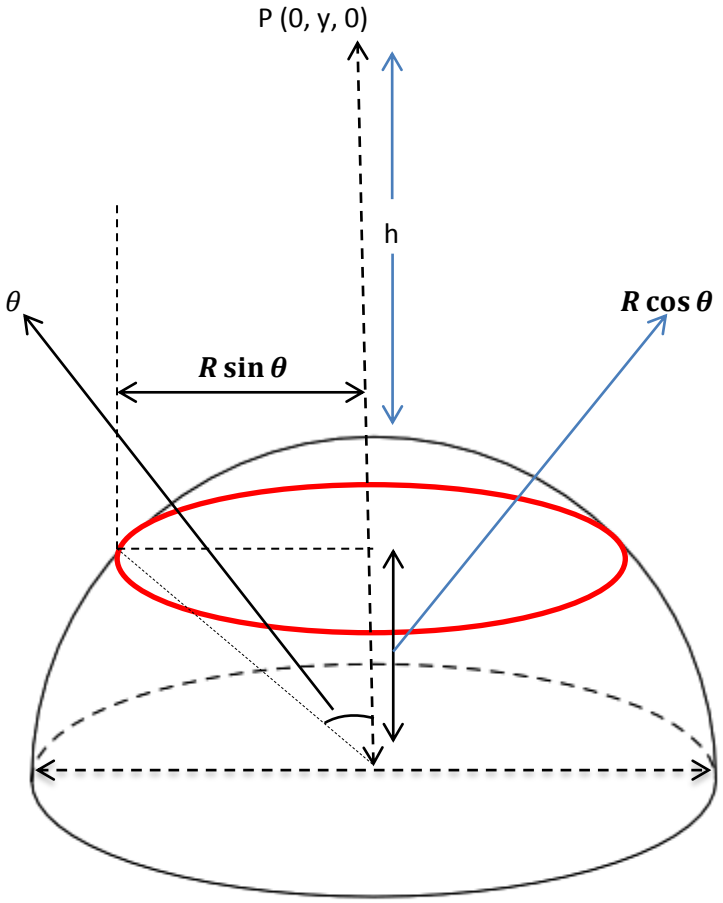

Fig. 4.3 Schematic diagram of hemispherical CNT tip -1

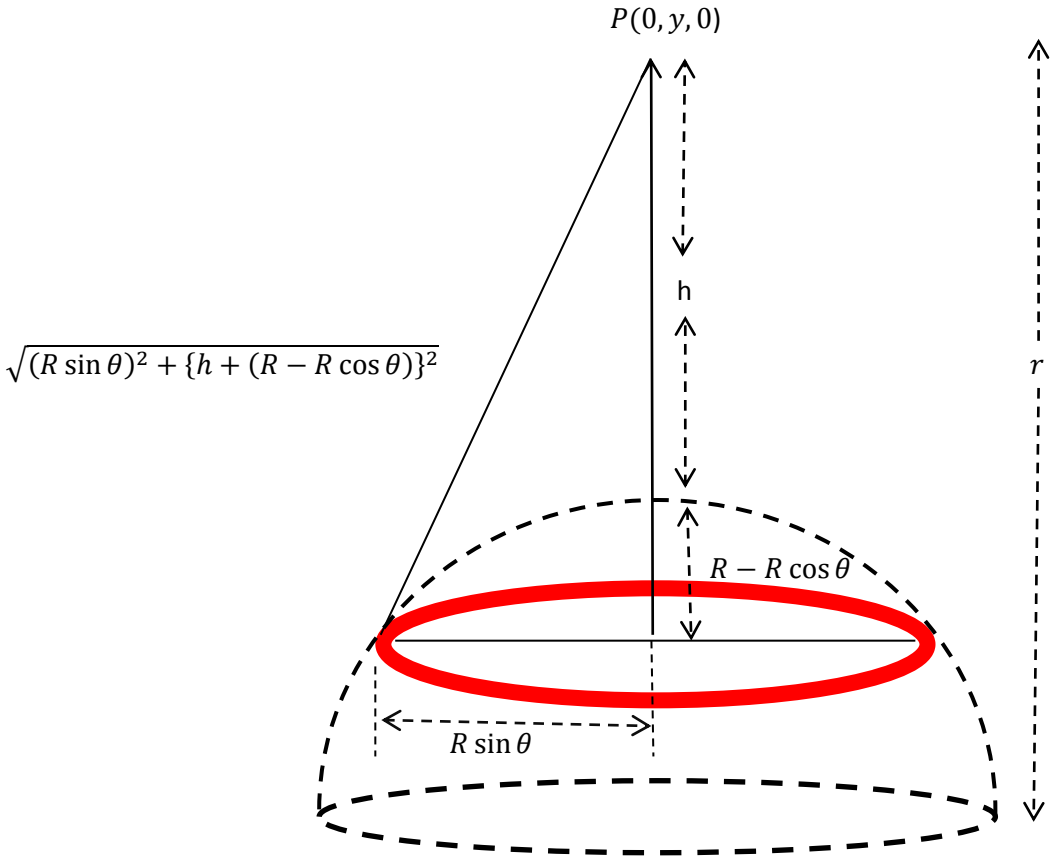

Fig. 4.4 Schematic diagram of hemispherical CNT tip -2

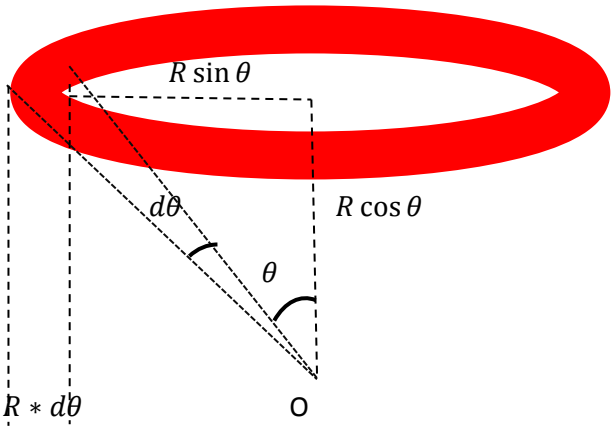

Fig. 4.5 Elementary Ring Charge

Let σ is the surface charge density.

Then charge on elemental strip will be .

$$dq = 2\pi R \sin\theta * Rd\theta * \sigma \ ,$$

We know that potential due to ring charge at any point will be,

$$dV = \frac{1}{4\pi\varepsilon_o}\frac{dq}{r}, \qquad (1)$$

where

$$r = \sqrt{\{(R\sin\theta)\}^2 + \{h + (R - R\cos\theta)\}^2}\ ,$$

$$dV = \frac{1}{4\pi\varepsilon_o} \quad \frac{2\pi R\sin\theta * R\ d\theta * \sigma}{\sqrt{\{(R\sin\theta)\}^2 + \{h + (R - R\cos\theta)\}^2}} \ ,$$

$$dV = \frac{1}{2\varepsilon_o} \quad \frac{R^2\sin\theta\sigma\ d\theta}{\sqrt{R^2sin^2\theta + h^2 + (R - R\cos\theta)^2 + 2h(R - R\cos\theta)}}\ ,$$

$$dV = \frac{1}{2\varepsilon_o} \quad \frac{R^2\sin\theta\sigma\ d\theta}{\sqrt{R^2sin^2\theta + R^2cos^2\theta + h^2 + R^2 - 2R^2cos\theta + 2hR(1 - \cos\theta)}},$$

$$dV = \frac{1}{2\varepsilon_o} \quad \frac{R^2\sin\theta\ \sigma\ d\theta}{\sqrt{R^2(\cos^2\theta + \sin^2\theta) + R^2 + h^2 - 2R^2cos\theta + 2hR(1 - \cos\theta)}}\ ,$$

$$dV = \frac{1}{2\varepsilon_o} \frac{R^2 \sin\theta\ \sigma\ d\theta}{\sqrt{2R^2+h^2-2R^2 cos\theta+2hR(1-\cos\theta)}} ,$$

$$dV = \frac{1}{2\varepsilon_o h} \frac{R^2 \sin\theta\ \sigma\ d\theta}{\sqrt{2\frac{R^2}{h^2}+1-2\frac{R^2}{h^2}\cos\theta+\frac{2R(1-\cos\theta)}{h}}} \quad (2)$$

Case:1

Electric Potential without Using Binomial Expression and excluding all power of $\frac{R}{h}$.

From Eq. (2),

$$dV = \frac{1}{2\varepsilon_o h} \frac{R^2 \sin\theta\ \sigma\ d\theta}{\sqrt{2\frac{R^2}{h^2}+1-2\frac{R^2}{h^2}\cos\theta+\frac{2R(1-\cos\theta)}{h}}} ,$$

Excluding all powers of $\frac{R}{h}$,

The expression will be ,

$$dV = \frac{1}{2\varepsilon_o h} \frac{R^2 \sin\theta\ \sigma\ d\theta}{1},$$

$$dV = \frac{R^2\sigma}{2\varepsilon_o h} sin\,\theta\ \ d\theta ,$$

Now we know that,

$$V = \int_0^{\frac{\pi}{2}} dV,$$

$$V = \int_0^{\frac{\pi}{2}} \frac{R^2\sigma}{2\varepsilon_o h} \sin\theta\ d\theta ,$$

$$V = \frac{R^2\sigma}{2\varepsilon_o h} \int_0^{\frac{\pi}{2}} \sin\theta\ d\theta ,$$

$$V = \frac{R^2\sigma}{2\varepsilon_o h} [-\cos\theta]_0^{\frac{\pi}{2}} ,$$

$$V = \frac{R^2\sigma}{2\varepsilon_o h},$$

We know that $\sigma = \frac{q}{2\pi R^2}$,

$$V = \frac{q}{4\pi\varepsilon_o h} \quad (3)$$

Case:2

Electric Potential without Using Binomial Expression and excluding higher power of $\frac{R}{h}$,

$$dV = \frac{1}{2\varepsilon_o h} \frac{R^2 \sin\theta\ \sigma\ d\theta}{\sqrt{2\frac{R^2}{h^2}+1-2\frac{R^2}{h^2}\cos\theta+\frac{2R(1-\cos\theta)}{h}}},$$

Excluding higher power of $\frac{R}{h}$,

$$dV = \frac{R^2\ \sigma}{2\varepsilon_o\ h} \frac{\sin\theta\ d\theta}{\sqrt{\left[1+2\frac{R}{h}(1-cos\theta)\right]}},$$

$$V = \int_0^{\frac{\pi}{2}} dV,$$

$$V = \frac{R^2\sigma}{2\varepsilon_o\ h}\int_0^{\frac{\pi}{2}} \frac{\sin\theta\ d\theta}{\sqrt{\left[1+\frac{2R}{h}(1-cos\theta)\right]}},$$

Let $1-\cos\theta = t$,

$$\sin\theta\, d\theta = dt,$$

Now the limit will be ,

θ	0	π/2
t	0	1

Let $2\frac{R}{h}$ = a,

$$V = \frac{R^2\sigma}{2\varepsilon_o h}\int_0^1 \frac{dt}{\sqrt{1+at}},$$

Let $= \frac{1}{a}$,

$$V = \frac{R^2\sigma}{2\varepsilon_o h}\int_0^1 \frac{dt}{a^{1/2}\sqrt{b+t}},$$

$$V = \frac{R^2\sigma}{2\varepsilon_o h}\,\frac{2}{a^{1/2}}\left[\sqrt{b+t}\right]_0^1,$$

$$V = \frac{R^2\sigma}{2\varepsilon_o h}\frac{2}{a}\left[\sqrt{at+1}\right]_0^1, \qquad \left[b = \frac{1}{a}\right]$$

$$V = \frac{R^2\sigma}{\varepsilon_o h}\frac{h}{2R}\left[\sqrt{a+1}-1\right],$$

$$V = \frac{\sigma R}{2\varepsilon_o}\left[\sqrt{\frac{2R}{h}+1}-1\right], \qquad \left[a = \frac{2R}{H}\right]$$

We know that $\sigma = \frac{q}{2\pi R^2}$,

Now

$$V = \frac{q}{4\pi\varepsilon_o R}\left(\sqrt{\frac{2R}{h}+1}-1\right) \qquad (4)$$

Case:3

Electric Potential By Using Binomial Expression and excluding only higher power of $\frac{R}{h}$,

Since h is in μm and R is in nm. We can ignore higher order of $\frac{R}{h}$,

$$\frac{R}{h} \approx 0,$$

$$dV = \frac{R^2\,\sigma}{2\varepsilon_o\,h}\ \frac{\sin\theta\ d\theta}{\sqrt{\left[1+2\frac{R}{h}(1-cos\theta)\right]}},$$

$$V = \int_0^{\frac{\pi}{2}} dV,$$

$$V = \frac{R^2\sigma}{2\varepsilon_o\,h}\int_0^{\frac{\pi}{2}} \frac{\sin\theta\ d\theta}{\sqrt{\left[1+\frac{2R}{h}(1-cos\theta)\right]}} \quad ,$$

$$V = \frac{R^2\sigma}{2\varepsilon_o\,h}\int_0^{\frac{\pi}{2}} \sin\theta\left\{1+\frac{2R}{h}(1-\cos\theta)\right\}^{-\frac{1}{2}} d\theta,$$

By using Binomial expression and again excluding higher power of $\frac{R}{h}$,

$$V = \frac{R^2\sigma}{2\varepsilon_o\,h}\int_0^{\frac{\pi}{2}} \sin\theta\left\{1-\frac{R}{h}(1-\cos\theta)\right\} d\theta,$$

Let $1-\cos\theta = t,$

$\sin\theta\ d\theta = dt,$

Now the Limit will be

θ	0	π/2
t	0	1

$$V = \frac{R^2\sigma}{2\varepsilon_o\, h}\int_0^1 \left(1 - \frac{R}{h}t\right) dt,$$

$$V = \frac{R^2\sigma}{2\varepsilon_o\, h}\left[t - \frac{t^2}{2}\frac{R}{h}\right]_0^1,$$

$$V = \frac{R^2\sigma}{2\varepsilon_o\, h}\left(1 - \frac{1}{2}\frac{R}{h}\right),$$

We know that $\sigma = \frac{q}{2\pi R^2}$,

Now ,

$$V = \frac{q}{4\pi\varepsilon_o h}\left[1 - \frac{R}{2h}\right],$$

$$V = \frac{q}{4\pi\varepsilon_o}\left[\frac{1}{h} - \frac{R}{2h^2}\right] \qquad (5)$$

In the above calculation we have derived three cases. For the calculation of Potential we will consider case 3. In case 3, during calculation we have excluded all possible higher orders of $\frac{R}{h}$. Radius of carbon nanotube will be in nanometer, and height will be in micro meter .So the ratio of radius to height will be approximately zero. In our model h is distance of point P (0, y, 0) from the tip of carbon nanotube. Latter we will replace *h* with *(r-R)*, where *r* is distance of point P (0 ,y ,0) from centre of hemispherical CNT tip.

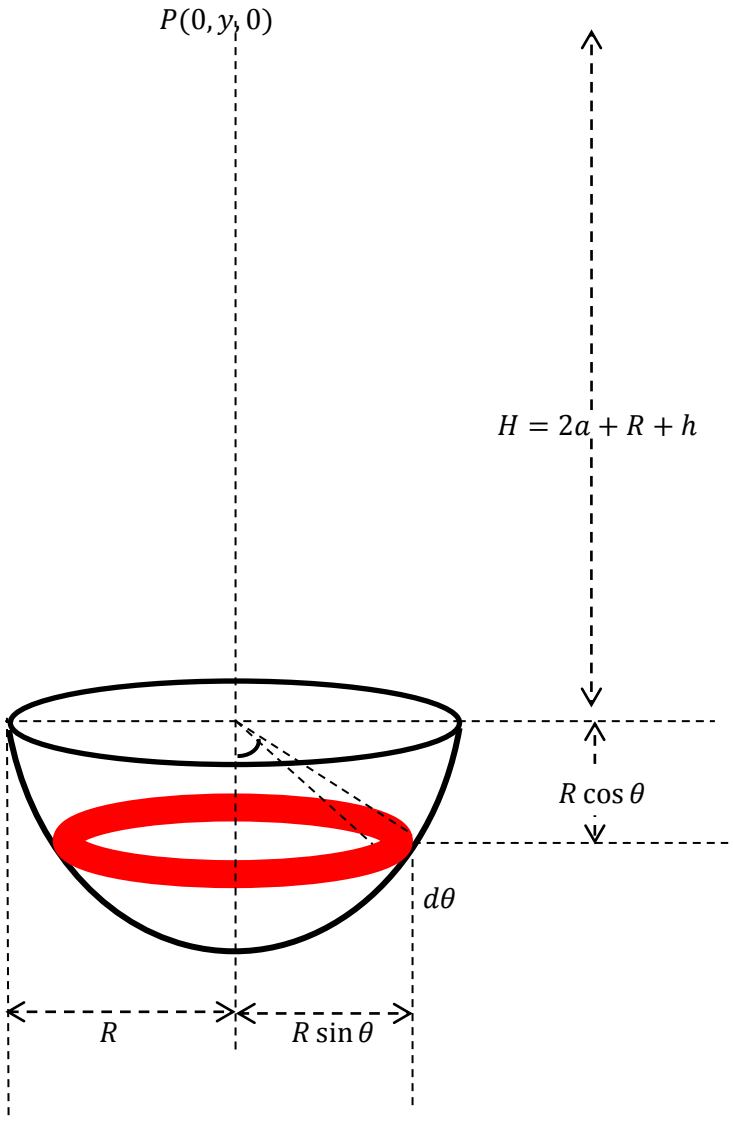

Fig. 4.6 Schematic diagram of hemispherical CNT image tip

The above diagram shows the image part of hemisphere. We will find out the potential at point P including image charge effect. So here first, we will find the potential due to image hemisphere V_{im} and then add it with hemisphere potential V.

To find out potential due to image hemisphere we will follow the same process as we have done for without image charge. We will consider image hemisphere into a infinitesimal ring charge.

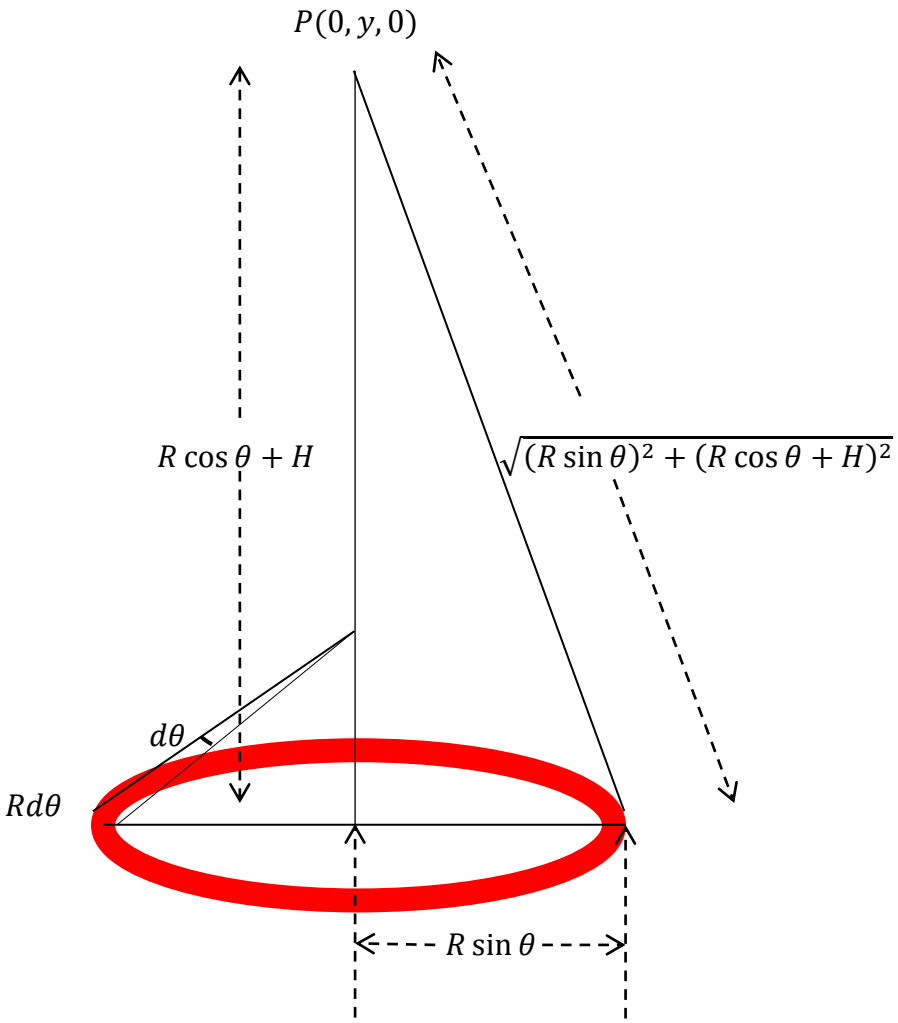

Fig. 4.7 Elementary ring charge

Let charge on elemental strip is dq.

Width of strip will be $Rd\theta$ as shown in the Fig. 4.7.

Periphery of strip will be $2\pi R\sin\theta$.

So the charge on elemental strip will be $dq = 2\pi R\sin\theta\, R\, d\theta\, \sigma$.

Let dV be potential due to elemental ring charge .

From Eq. (1) , potential due to elemental ring charge can be written as,

$$dV_{im} = -\frac{2\pi R\sin\theta R\, d\theta\, \sigma}{4\pi\varepsilon_o}\frac{1}{\sqrt{(R\sin\theta)^2+(R\cos\theta+H)^2}},$$

$$dV_{im} = -\frac{R^2\sin\theta\, d\theta\, \sigma}{2\varepsilon_o}\frac{1}{\sqrt{R^2sin^2\theta+R^2cos^2\theta+2RH\cos\theta+H^2}},$$

$$dV_{im} = -\frac{R^2 \sin\theta \, d\theta \, \sigma}{2\varepsilon_o} \frac{1}{\sqrt{R^2+2RH\cos\theta+H^2}},$$

$$dV_{im} = -\frac{R^2 \sin\theta \, d\theta \, \sigma}{2\varepsilon_o H} \frac{1}{\sqrt{\frac{R^2}{H^2}+\frac{2R\cos\theta}{H}+1}},$$

Since H is in μm/mm and R is in nm so we can ignore higher order of $\frac{R}{h}$

$$\frac{R}{h} \approx 0,$$

$$dV_{im} = -\frac{R^2 \sin\theta \, d\theta \, \sigma}{2\varepsilon_o H} \frac{1}{\sqrt{\frac{2R\cos\theta}{H}+1}},$$

Potential at point P due to image charge will be

$$V_{im} = \int_0^{\frac{\pi}{2}} dV_{im},$$

$$V_{im} = -\frac{R^2\sigma}{2\varepsilon_o H} \int_0^{\frac{\pi}{2}} \frac{\sin\theta \, d\theta}{\sqrt{1+\frac{2R\cos\theta}{H}}},$$

$$V_{im} = -\frac{R^2\sigma}{2\varepsilon_o H} \int_0^{\frac{\pi}{2}} \sin\theta \left[1+\frac{2R}{H}\cos\theta\right]^{-\frac{1}{2}} d\theta,$$

By using binomial expression

$$V_{im} = -\frac{R^2\sigma}{2\varepsilon_o H} \int_0^{\frac{\pi}{2}} \sin\theta \left[1-\frac{1}{2}\frac{2R}{H}\cos\theta\right] d\theta,$$

$$V_{im} = -\frac{R^2\sigma}{2\varepsilon_o H} \left[\left[\int_0^{\frac{\pi}{2}} \sin\theta \, d\theta\right] - \frac{R}{H}\left[\int_0^{\frac{\pi}{2}} \sin\theta\cos\theta \, d\theta\right]\right],$$

$$V_{im} = -\frac{R^2\sigma}{2\varepsilon_o H}\left[[-\cos\theta]_0^{\frac{\pi}{2}} - \frac{R}{2H}\left[\int_0^{\frac{\pi}{2}} \sin 2\theta \, d\theta\right]\right],$$

$$V_{im} = -\frac{R^2\sigma}{2\varepsilon_o H}\left[1 - \frac{R}{2H}\frac{1}{2}[-\cos 2\theta]_0^{\frac{\pi}{2}}\right],$$

$$V_{im} == -\frac{R^2\sigma}{2\varepsilon_o H}\left[1 - \frac{R}{2H}\right],$$

We know that the charge density for hemisphere $\sigma = \frac{q}{2\pi R^2}$,

$$V_{im} = -\frac{q}{4\pi\varepsilon_o H}\left[1 - \frac{R}{2H}\right], \quad (6)$$

where $H = 2a + R + h = 2a + r$,

From equation (5) and (6),

The potential of hemispherical CNT tip including image charge effect will be given by

$$V_{total} = V + V_{im},$$

$$V_{total} = \frac{\mathrm{q}}{4\pi\varepsilon_o}\left[\frac{1}{\mathrm{h}} - \frac{\mathrm{R}}{2\mathrm{h}^2}\right] - \frac{\mathrm{q}}{4\pi\varepsilon_o \mathrm{H}}\left[1 - \frac{\mathrm{R}}{2\mathrm{H}}\right],$$

In CGS,

$$V_{total} = \frac{q}{h}\left[1 - \frac{R}{2h^2}\right] - \frac{q}{H}\left[1 - \frac{R}{2H}\right], \quad (7)$$

Fig. 4.8 represents carbon nanotube with hemispherical tip including image charge.

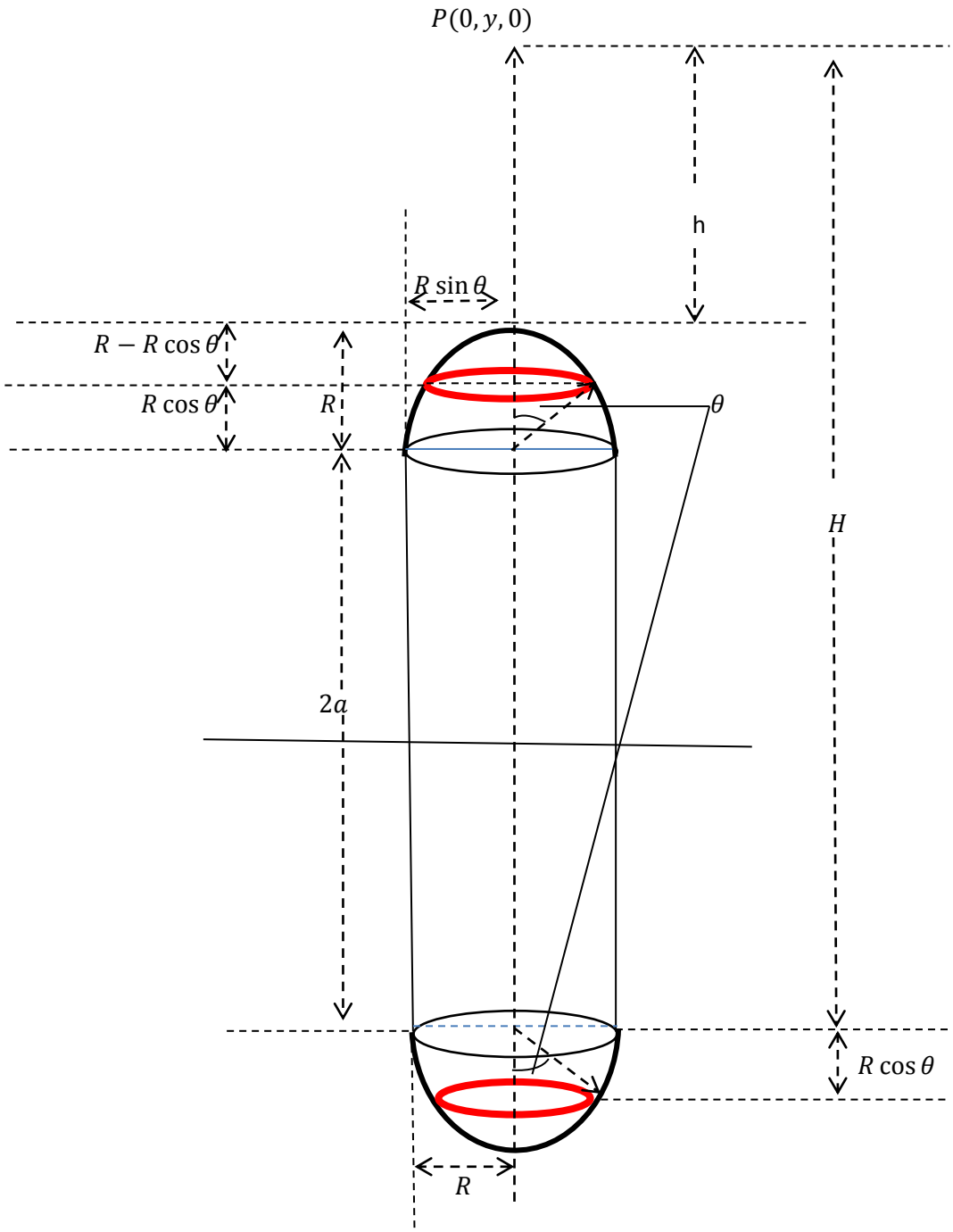

Fig. 4.8 Electrostatic model for CNT including image charge effect

The potential energy shown by eq. (7) does not contain barrier height. After consideration of barrier height the potential of hemispherical CNT tip including image charge effect will be

$$V(r) = \frac{q^2}{h}\left[1 - \frac{R}{2h}\right] - \frac{q^2}{H + \frac{q^2}{W_a}}\left[1 - \frac{R}{2H}\right], \quad (8)$$

where w_a is barrier height.

By replacing the value of $h = r - R \;\; \& \;\; H = 2a + r$ in Eq. (8) the potential energy will be

$$V(r) = \frac{\mathrm{q}^2}{(\mathrm{r}-\mathrm{R})}\left[1 - \frac{\mathrm{R}}{2(\mathrm{r}-\mathrm{R})}\right] - \frac{\mathrm{q}^2}{(2\mathrm{a}+\mathrm{r})+\frac{q^2}{W_a}}\left[1 - \frac{\mathrm{R}}{2(2\mathrm{a}+\mathrm{r})}\right]$$

The graph shown below represents the potential of hemispherical CNT tip including image charge effect.

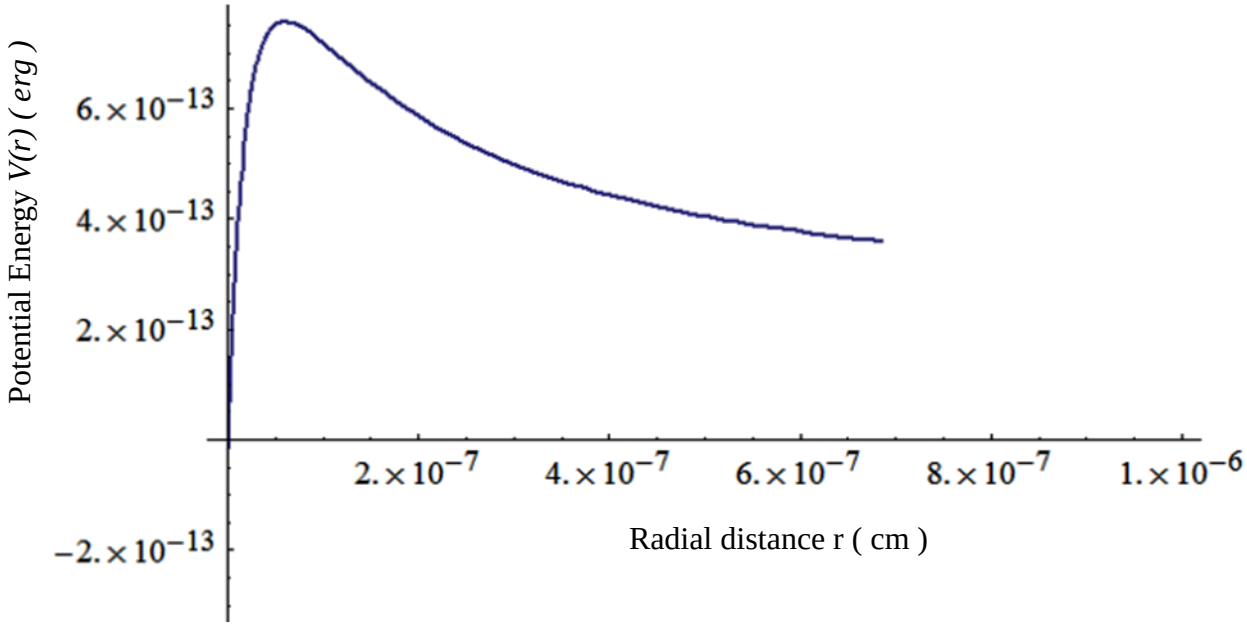

Fig. 4.9 Variation of potential energy, *V(r)*, with radial distance *r* for $r > R$

The time independent schrodinger wave equation in the region $r > R$, including the image force is given by

$$\nabla^2\psi(r,\theta,\phi) + \frac{2m_e}{\hbar^2}\left[E + \frac{\mathrm{q}^2}{(2\mathrm{a}+\mathrm{r})+\frac{q^2}{W_a}}\left[1 - \frac{\mathrm{R}}{2(2\mathrm{a}+\mathrm{r})}\right] - \frac{\mathrm{q}^2}{(\mathrm{r}-\mathrm{R})}\left[1 - \frac{\mathrm{R}}{2(\mathrm{r}-\mathrm{R})}\right]\right]\psi(r,\theta,\phi) = 0, \quad (9)$$

where $\hbar$ is $h/2\pi$, h being Planck's constant; m_e is the mass of the electron, $\psi(r,\theta,\phi)$ is the wave function associated with the electrons emitted from the spherical conducting CNT, including the image force. The term $\frac{q^2}{W_a}$ in the denominator of the second term may be neglected for our case because it is unimportant except in the immediate vicinity of the

surface , and we are only considering r > R. Using separation of variables to separate the radial and angular terms of the wave equation, we can write

$$\psi(r,\theta,\phi) = R(r)Y(\theta,\phi) = \frac{U(r)}{r}Y(\theta,\phi) \ , \tag{10}$$

$$\frac{d^2U(r)}{dr^2} + \frac{2m_e}{\hbar^2}\left[E + \frac{\mathrm{q}^2}{(2\mathrm{a}+\mathrm{r})}\left(1 - \frac{\mathrm{R}}{2(2\mathrm{a}+\mathrm{r})}\right) - \frac{\mathrm{q}^2}{(\mathrm{r}-\mathrm{R})}\left(1 - \frac{\mathrm{R}}{2(\mathrm{r}-\mathrm{R})}\right) - \frac{\hbar^2}{2m_e r^2}l(l+1)\right]U(r)=0, \tag{11}$$

In the above equation we have ignored the barrier term becaues its effect will be zero.

Substituting

$$E - \frac{\hbar^2}{2m_e r^2}l(l+1) = E_r \ , \tag{12}$$

Eq. (11) can be rewritten as

$$\frac{d^2U(r)}{dr^2} + \frac{2m_e}{\hbar^2}\left[E_r + \frac{\mathrm{q}^2}{(2\mathrm{a}+\mathrm{r})}\left(1 - \frac{\mathrm{R}}{2(2\mathrm{a}+\mathrm{r})}\right) - \frac{\mathrm{q}^2}{(\mathrm{r}-\mathrm{R})}\left(1 - \frac{\mathrm{R}}{2(\mathrm{r}-\mathrm{R})}\right)\right]U(r)=0, \tag{13}$$

or

$$\frac{d^2U(r)}{dr^2} + \frac{2m_eV_oR^2}{\hbar^2}\left[\frac{E_\rho}{V_o} + \frac{\mathrm{q}^2}{(2\mathrm{a}+\mathrm{r})V_o}\left(1 - \frac{\mathrm{R}}{2(2\mathrm{a}+\mathrm{r})}\right) - \frac{\mathrm{q}^2}{(\mathrm{r}-\mathrm{R})V_o}\left(1 - \frac{\mathrm{R}}{2(\mathrm{r}-\mathrm{R})}\right)\right]U(\rho)=0, \tag{14}$$

Normalizing the above equation using $\rho = \frac{r}{R}$, $k = \frac{2a}{R}$,

$$\frac{d^2U(\rho)}{d\rho^2} + \frac{2m_eV_oR^2}{\hbar^2}\left[\frac{E_\rho}{V_o} + \frac{\mathrm{q}^2}{\mathrm{R}(\mathrm{k}+\rho)V_o}\left(1 - \frac{1}{2(\mathrm{k}+\rho)}\right) - \frac{\mathrm{q}^2}{\mathrm{R}(\rho-1)V_o}\left(1 - \frac{1}{2(\rho-1)}\right)\right]U(\rho)=0, \tag{15}$$

Let

$$\frac{2m_eV_oR^2}{\hbar^2} = \beta_2 \ , \tag{16}$$

$$\frac{E_\rho}{V_o} = \varepsilon_\rho \ , \tag{17}$$

$$\frac{q^2}{V_o 4\pi\varepsilon_o R} = \beta_1 \ , \tag{18}$$

$$\frac{d^2U(\rho)}{d\rho^2} + \beta_2\left[\varepsilon_\rho + \frac{\beta_1}{(k+\rho)}\left(1 - \frac{1}{2(k+\rho)}\right) - \frac{\beta_1}{(\rho-1)}\left(1 - \frac{1}{2(\rho-1)}\right)\right]U(\rho)=0, \quad (19)$$

$$\frac{d^2U(\rho)}{d\rho^2} + \Gamma^2 U(\rho) = 0\ , \quad (20)$$

where

$$\Gamma^2 = \beta_2\left[\varepsilon_\rho + \frac{\beta_1}{(k+\rho)}\left(1 - \frac{1}{2(k+\rho)}\right) - \frac{\beta_1}{(\rho-1)}\left(1 - \frac{1}{2(\rho-1)}\right)\right], \quad (21)$$

Electron transmission coefficient

The probability of electron tunnelling, $T(\varepsilon_\rho)$, from the spherical conducting CNT, including the image charge force and using JWKB [29] approximation can be given as

$$T(\varepsilon_\rho) = \exp\left(-2\int_{\rho_1}^{\rho_2}\sqrt{-\Gamma^2}\,d\rho\right) \quad , \quad (22)$$

for $r > R$

Now we will calculate the value of transmission coefficient for different radius.
Here $m_e = 9.1094 \times 10^{-28} gm,$

$$V_o = 5eV = 5 \times 1.6 \times 10^{-12} erg,$$

$$\hbar = 1.0546 \times 10^{-27} erg - sec\ ,$$

1. **For R= 0.5 nm**

$$\beta_1 = .567,$$
$$\beta_2 = 32.799,$$

Radial energy ε_ρ	**Transmission coefficient** $T(\varepsilon_\rho)$
0.01	0.0661
0.015	0.0682
0.02	0.0703
0.025	0.0725
0.03	0.0748
0.035	0.0772

Table.1. Radial Energy and Transmission coefficient (R=0.5nm)

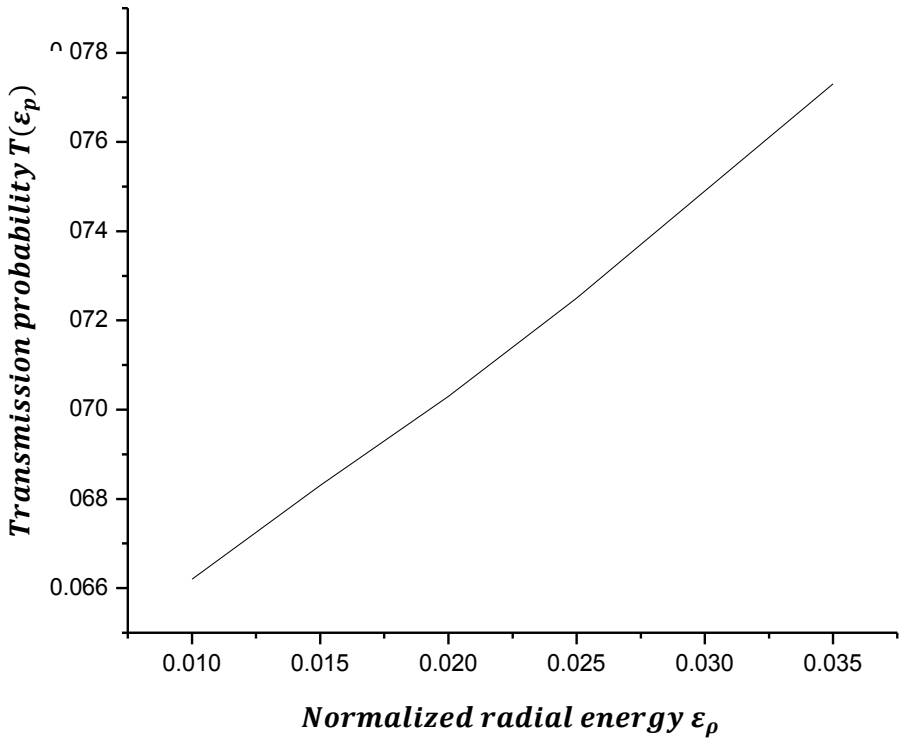

Fig. 4.10 Transmission coefficient as function of normalized radial energy for R=.5nm

1. **For R= 1 nm**

$\beta_1 = .288,$

$\beta_2 = 131.198$,

Radial energy ε_ρ	**Transmission coefficient** $T(\varepsilon_\rho)$
0.01	0.0234
0.015	0.0256
0.02	0.0280
0.025	0.0307
0.03	0.0338
0.035	0.0372

Table.2. Radial Energy and Transmission coefficient (R=1nm)

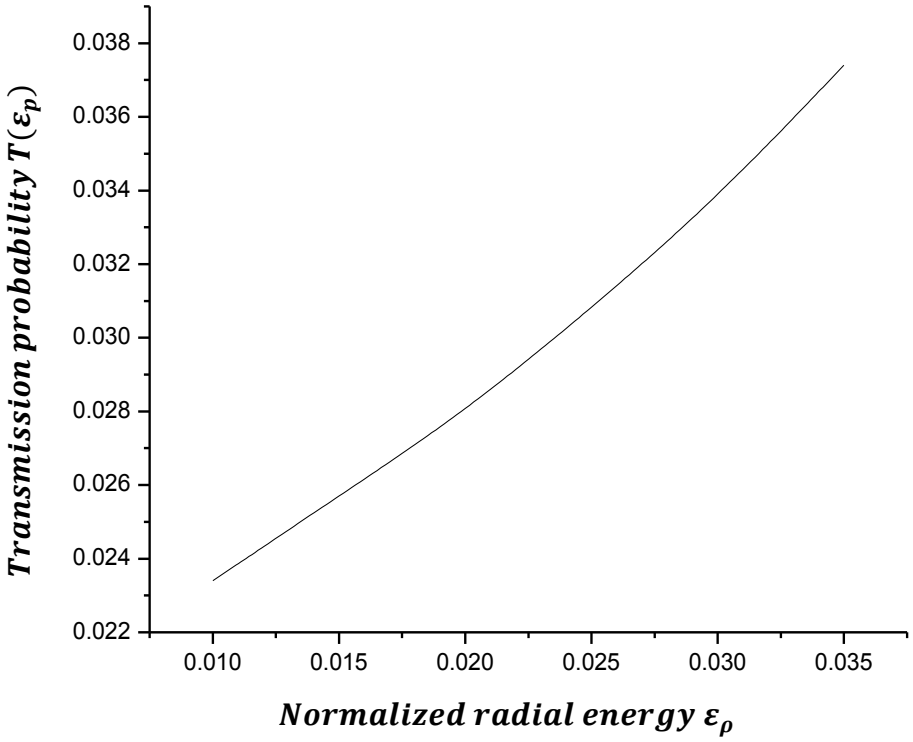

Fig. 4.11 Transmission coefficient as function of normalized radial energy for R=1nm

2. For R= 1.5 nm

$\beta_1 = .192,$

$\beta_2 = 295.1955$,

Radial energy ε_ρ	**Transmission coefficient** $T(\varepsilon_\rho)$
0.01	0.0112
0.015	0.0133
0.02	0.0158
0.025	0.0189
0.03	0.0230
0.035	0.0280

Table.3. Radial Energy and Transmission coefficient (R=1.5nm)

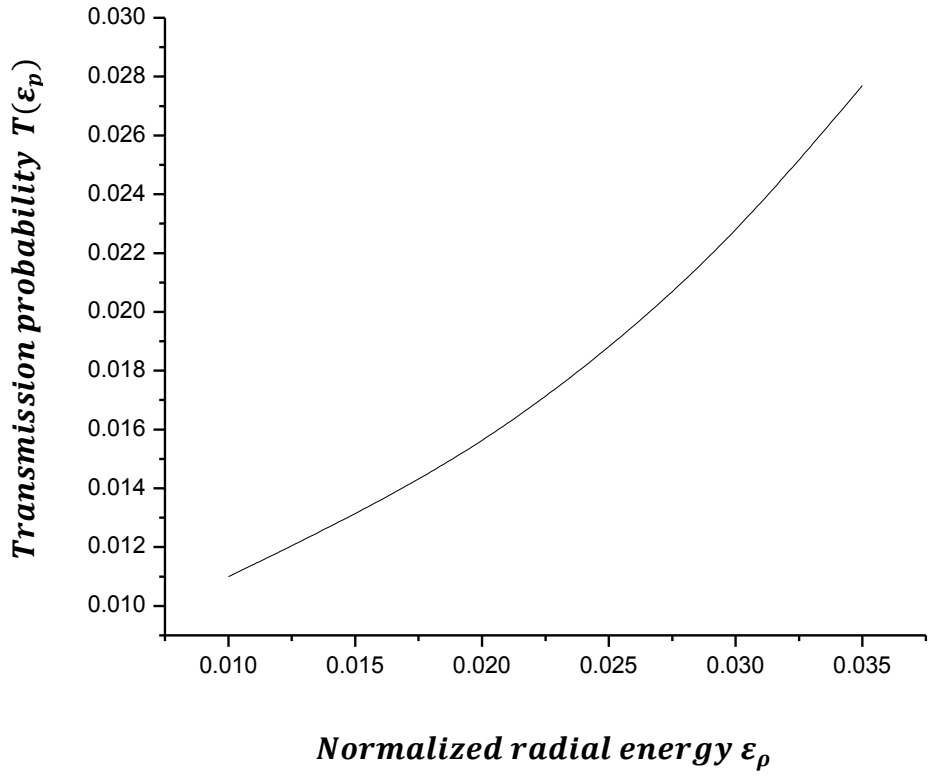

Fig. 4.12 Transmission coefficient as function of normalized radial energy for R=1.5nm

3. For R= 2 nm

$\beta_1 = .144,$

$\beta_2 = 524.792,$

Radial energy ε_ρ	**Transmission coefficient** $T(\varepsilon_\rho)$
0.01	0.00636
0.015	0.008306
0.02	0.011019
0.025	0.0149
0.03	0.0206
0.035	0.0274

Table.4. Radial Energy and Transmission coefficient (R=2nm)

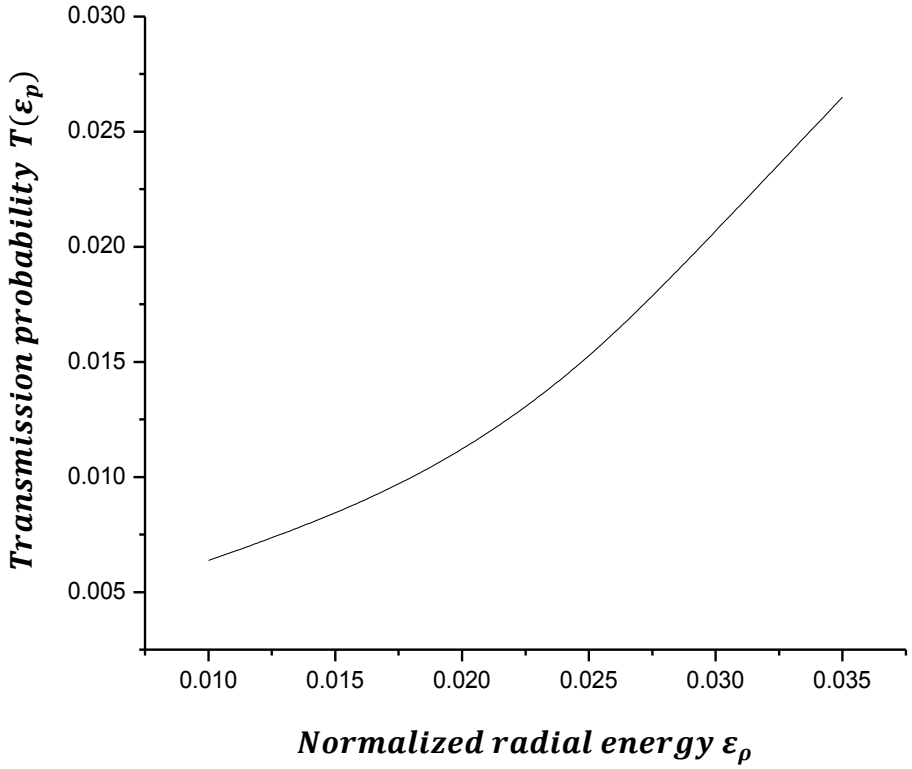

Fig. 4.13 Transmission coefficient as function of normalized radial energy for R=2nm

Field Emission Current & Current Density function

Field emission current is also known as cold cathode emission current, as it is the current due to the electron that can be emitted from the cathode, even when the temperature of the cathode is $0\ K$. Hence, the field emission current density [31] at $0\ K$ is given as

$$J\left(\varepsilon_p, \varepsilon_f, T(\varepsilon_\rho)\right) = \frac{4\pi m_e e}{\hbar^3} V_o^2 \int_0^{\varepsilon_f} \left(\varepsilon_f - \varepsilon_\rho\right) T(\varepsilon_\rho) d\varepsilon_\rho, \tag{23}$$

Here the current density J, is the function of normalized radial energy, ε_ρ; normalized Fermi energy, ε_f; and the transmission coefficient. More-over the current density function, ϕ, is given as

$$\phi = \int_0^{\varepsilon_f} \left(\varepsilon_f - \varepsilon_\rho\right) T(\varepsilon_\rho) d\varepsilon_{\rho,} \tag{24}$$

Now, we have to show that the current density function for different value of hemisphere radius

For R= 0.5 nm

Current density function ϕ_1 is given as

$$\phi_1 = \int_0^{\varepsilon_f} (\varepsilon_f - \varepsilon_\rho)\, T_1(\varepsilon_\rho) d\varepsilon_\rho,$$

Here , $T_1(\varepsilon_\rho)$ is the transmission probability obtained from table 1

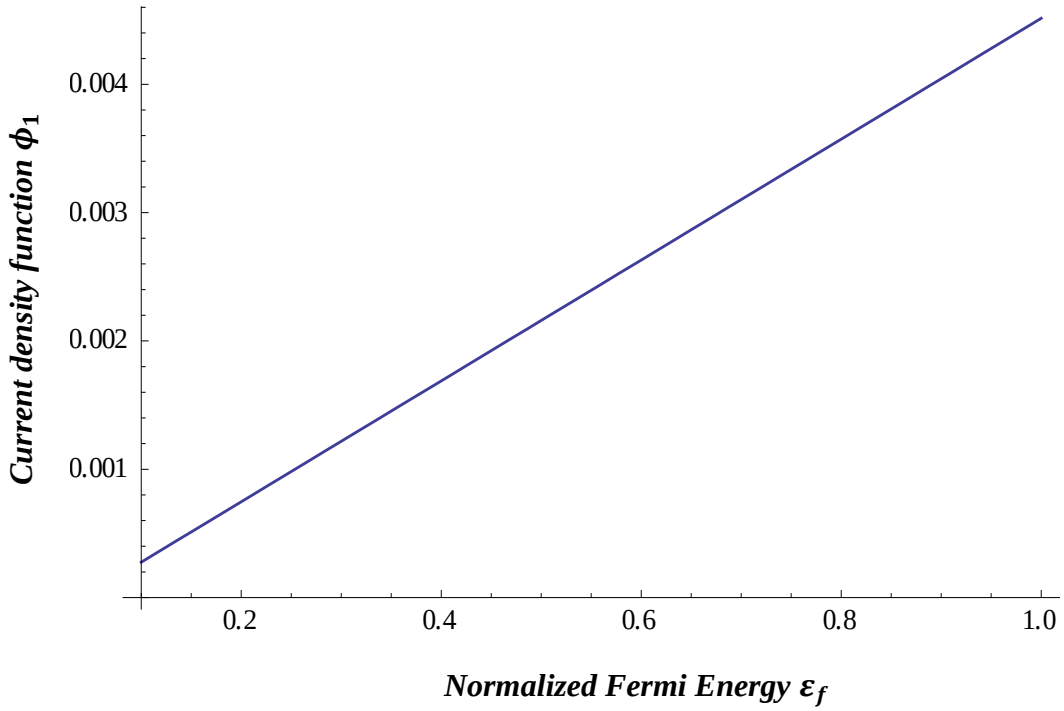

Fig. 4.14 Variation of current density function with normalized Fermi energy for R=.5nm

For R= 1 nm

Current density function ϕ_2 is given as

$$\phi_2 = \int_0^{\varepsilon_f} (\varepsilon_f - \varepsilon_\rho)\, T_2(\varepsilon_\rho) d\varepsilon_{\rho,},$$

Here , $T_2(\varepsilon_\rho)$ is the transmission probability obtained from table 2

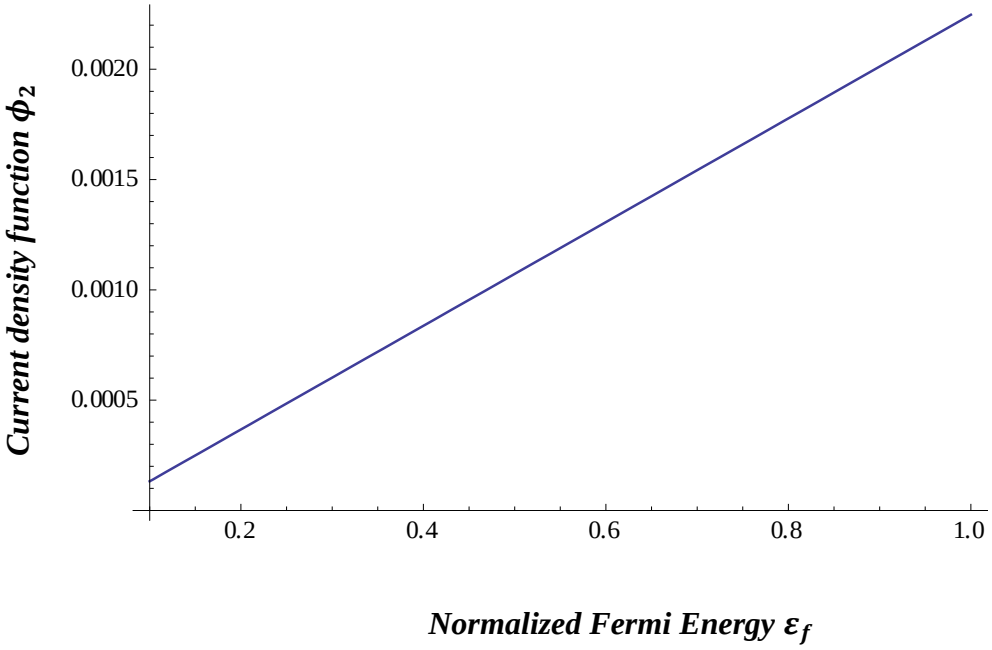

Fig. 4.15 Variation of current density function with normalized Fermi energy R=1nm

For R= 1.5 nm

Current density function ϕ_3 is given as

$$\phi_3 = \int_0^{\varepsilon_f} (\varepsilon_f - \varepsilon_\rho)\, T_3(\varepsilon_\rho) d\varepsilon_\rho,$$

Here , $T_3(\varepsilon_\rho)$ is the transmission probability obtained from table 3

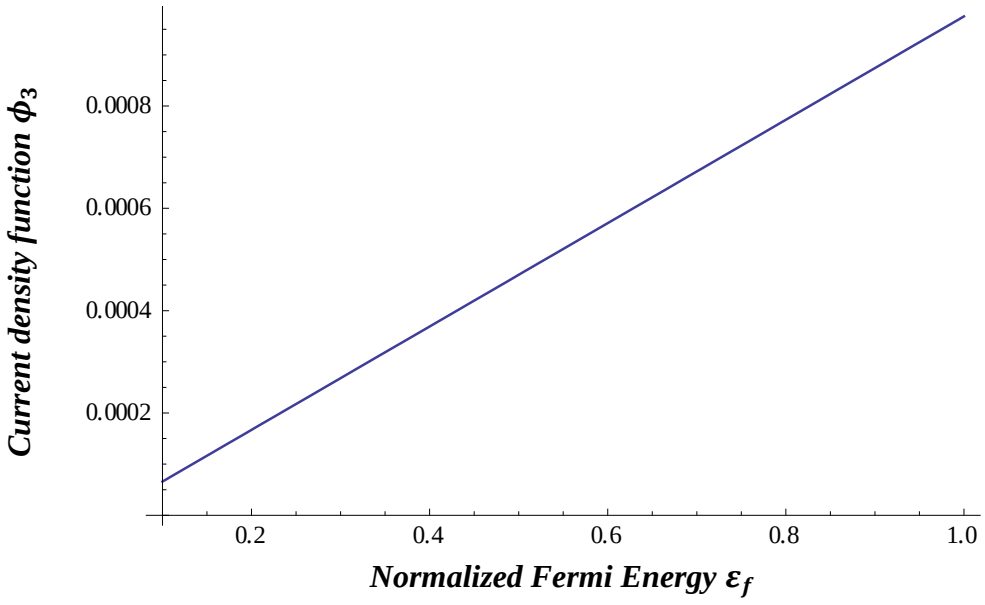

Fig. 4.16 Variation of current density function with normalized Fermi energy for R=1.5nm.

For R= 2 nm

Current density function ϕ_4 is given as

$$\phi_4 = \int_0^{\varepsilon_f} (\varepsilon_f - \varepsilon_\rho)\, T_4(\varepsilon_\rho) d\varepsilon_\rho,$$

Here , $T_4(\varepsilon_\rho)$ is the transmission probability obtained from table 4

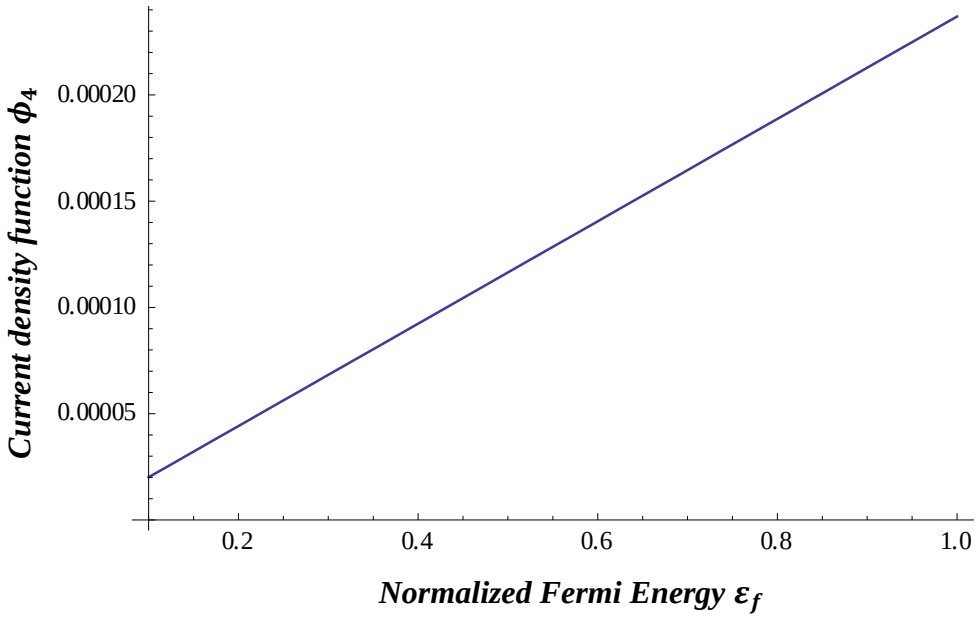

Fig. 4.17 Variation of current density function with normalized Fermi energy for R=2nm.

Chapter 5

Results and discussion

5.1 Results and discussion

In the calculation we have evaluated various parameters like potential energy, tunnelling probability and the field emission current density by using various CNT parameters. Variation of potential energy *V(r)* (in ergs) of emitted electron as a function of radial distance, *r* (in nm) from the hemispherical CNT tip including image charge effect is shown in figure 4.9. It is clear from figure 4.9 that the potential energy of emitted electron first increases with radial distance r and then decreases. Because of image force potential is increasing initially. Using Eq. (22) we have evaluated transmission coefficient as function of normalized radial energy for different radius (e.g. ,R=0.5 nm, 1 nm, 1.5 nm, 2 nm) . From **Figs. 4.10, 4.11, 4.12 and 4.13** we can say that the probability of electron tunnelling increases with normalized radial energy.

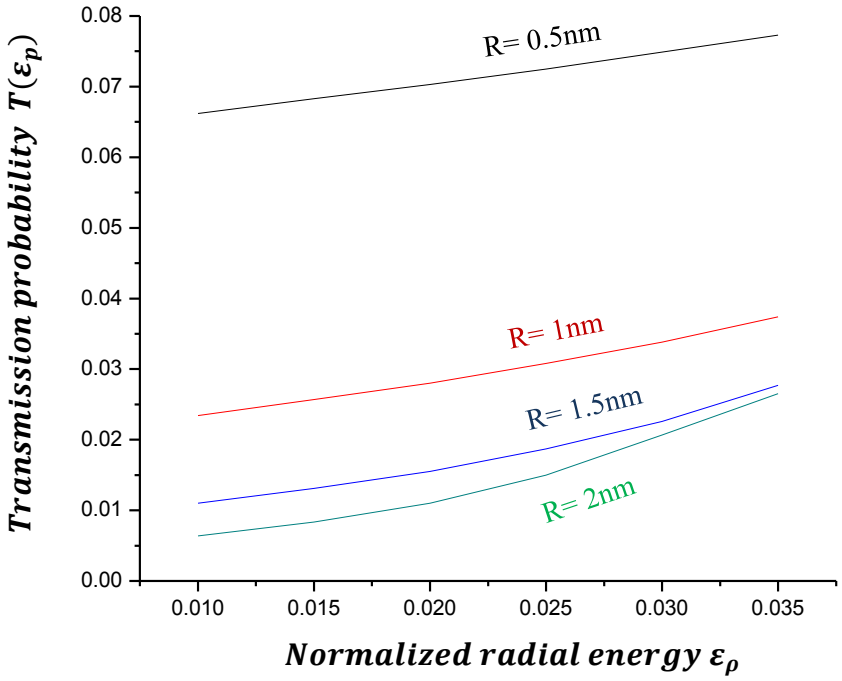

Fig. 5.1 Comparison of Transmission probability for different hemispherical radius

From Fig. 5.1 we can say that the electron tunnelling probability decreases as radius of hemispherical CNT tip increased. Using Eq.(24), we have plotted in Fig. 5.2, the current

density function as a function of normalized fermi energy in presence of image charge for different radius of hemispherical tip; R = 0.5,1, 1.5 and 2 nm, respectively. From fig 5.2 we can say that the current density function increases with normalized Fermi energy, and field emission current density function decreases when the tube radius is increased as reported by Zhou et al. [13]. Hence, our theoretical results are qualitatively similar to experimental observation of Zhou et al. [13] and Xu et al. [32].

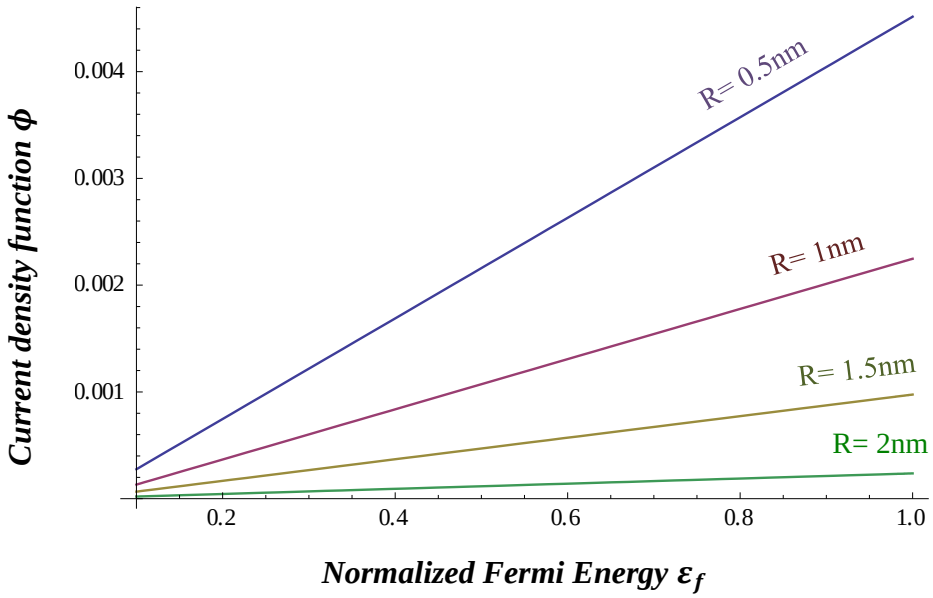

Fig. 5.2 Comparison of current density functions for different hemispherical radius

From Fig. 5.2 Following considerable effect due to image force :

1. The applied electric field is reduced and appreciably larger than normal value of the electron transmission probability
2. The current density functions are obtained at lower fields.

Chapter 6

Conclusion

In conclusion, we may say that the transmission probability of electrons emitted from hemispherical CNTs tip, increases with normalized radial energy. Field emission current density of electrons from the hemispherical CNT tip also increases with Fermi energy. It is also observed that the transmission probability and the field emission current density decrease with hemispherical tip radius. Due to consideration of the image force, the applied field reduces. This is a profitable condition in experiments, that at lower fields higher emissions of electrons is obtained. The current observation has also been experimentally reported by Gomer [33] and Fowler and Nordheim [34].

REFERENCE

[1] S. C. Sharma and A. Tewari, Can. J. Phys. **89,** 875 (2011).

[2] P. K. Dubey, J. Phys. D: J. Appl. Phys. **3**, 145 (1970).

[3] M. S. Sodha, A. Dixit, and S. K. Agarwal, Can. J. Phys. **87**, 175 (2009).

[4] J. M. Bonard, J. P. Salvetat, T. Stockli, W. A. de Heer, L. Forró, and A. Châtelain. Appl Phys. Lett. **73**, 918 (1998).

[5] W. Zhu, C. Bower, O. Zhou, G. Kochanski, and S. Jin. Appl. Phys. Lett. **75**, 873 (1999).

[6] D. Y. Zhong, G. Y. Zhang, S. Liu, T. Sakurai, and E. G. Wang, Appl. Phys. Lett. **80**, 506 (2002).

[7] L. Nilsson, O. Groening, C. Emmenegger, O. Kuettel, E. Schaller, L. Schlapbach, H. Kind, J.-M. Bonard, and K. Kern, Appl. Phys. Lett. **76**, 2071 (2000).

[8] L. H. Chan, K. H. Hong, D. Q. Xiao, W. J. Hsieh, S. H. Lai, H. C. Shih, T. C. Lin, F. S. Shieu, K. J. Chen, and H. C. Cheng, Appl. Phys. Lett. **82**, 4334 (2003).

[9] X. Q. Wang, M. Wang, P. M. He, Y. B. Xu, and Z. H. Li, J. Appl. Phys. **96**, 6752 (2004).

[10] R. C. Smith, J. D. Carey, R. D. Forrest, and S.R.P. Silva, J. Vac. Sci. Technol. B, **23**, 632 (2005).

[11] A. Ahmad and V. K. Tripathi, Nanotechnology, **17**, 3798 (2006).

[12] G. Zhang, W. Duan, and B. Gu, Appl. Phys. Lett. **80**, 2589 (2002).

[13] G. Zhou, W. Duan, and B. Gu, Appl. Phys. Lett. **79**, 836 (2001).

[14] J. Luo, L. M. Peng, Z.Q. Xue, and J. L. Wu, Phys. Rev. **66**, 155407 (2002).

[15] S. Han and J. Ihm, Phys. Rev. B, **61**, 9986 (2000).

[16] Y. H. Lee, C. H. Choi, Y. T. Jang, E. K. Kim, B. K. Ju, N. K. Min, and J. H. Ahn, Appl. Phys. Lett. **81**, 745 (2002).

[17] J. S. Suh, K.S. Jeong, J.S. Lee, and I. Han, Appl. Phys. Lett. **80**, 2392 (2002).

[18] J. M. Bonard, C. Klinke, K. Dean, and B. Coll, Phys. Rev. B, **67**, 115406 (2003).

[19] S. H. Jo, Y. Tu, Z.P. Huang, D. L. Carnahan, D. Z. Wang, and Z. F. Ren, Appl. Phys. Lett. **82**, 3520 (2003).

[20] R. C. Che, L. M. Peng, and M. S. Wang, Appl. Phys. Lett. **85**, 4753 (2004).

[21] S. K. Srivastava, A. K. Shukla, V. D. Vankar, and V. Kumar. Thin Solid Films, **492**, 124 (2005).

[22] S. K. Srivastava V. D. Vankar, D. V. Sridhar Rao, and V. Kumar, Thin Solid Films, **515**, 1851 (2006).

[23] S. K. Srivastava, V. D. Vankar, and V. Kumar, Nanoscale Res. Lett. **3**, 25 (2008).

[24] X. Ma and E. G. Wang, Appl. Phys. Lett. **78**, 978 (2001).

[25] J. Y. Lee and B. S. Lee, Thin Solid Films, **418**, 85 (2002).

[26] T. Kato, G. H. Jeong, T. Hirata, R. Hatakeyama, K. Tohji, and K. Motomiya, Chem. Phys. Lett. **381**, 422 (2003).

[27] S.B. Lee, A.S. Teh, K.B.K. Teo, M. Chhowalla, D.G. Hasko, W.I. Milne, G.A.J. Amaratunga, and H. Ahmed. Nanotechnology, 14, 192 (2003).

[28] F. Lee, Y.P. Chang, and L.Y. Lee. J. Mater. Sci. Mater.Electron. 20, 851 (2009).

[29] A. Ghatak and S. Lokanathan. Quantum Mechanics: Theory and Applications. 5^{th} Ed. Macmillan Publishers India Ltd. 2009.

[30] M. S. Sodha and S. Sharma, Br. J. Appl. Phys. **18**, 1127 (1967).

[31] F. Seitz, Modern Theory of Solids. McGraw-Hill, New York.1940.

[32] Z. Xu, X. D. Bai, and E.G. Wang, Appl. Phys. Lett. **88**, 133107 (2006).

[33] R. Gomer, *Field Emission and Field Ionization*. American Institute of Physics, (NewYork. 1993).

[34] R. H. Fowler and L.W. Nordheim, Proc. R. Soc. Lond. A119, 173 (1928).